# Angular dependence and polarization of out-of-plane optical scattering from particulate contamination, subsurface defects, and surface microroughness

Thomas A. Germer

The angular dependence and the polarization of light scattered by a small particle a distance $d$ inside and outside a reflecting surface is calculated in the Rayleigh limit. This calculation yields expressions for the polarized bidirectional reflectance distribution function matrices for in-plane and out-of-plane scattering. The results are compared with those obtained from microroughness-induced scattering. For the $p$-in/$p$-out configuration with oblique incidence, there exist out-of-plane angles for which scattering that is due to one of the mechanisms vanishes, whereas that from the others does not. By exploiting this knowledge, we can make improvements in the detection of small particles or subsurface defects. It is also shown that one must take care when differentiating subsurface-defect-induced scattering from microroughness-induced scattering using in-plane scattering and wavelength scaling laws.

*Key words:* Bidirectional reflectance distribution function, polarimetry, particulate contamination, subsurface defects, microroughness.

## 1. Introduction

Optical scattering is often a powerful tool for *in situ* process monitoring in manufacturing environments because of its noncontact nature and its relative ease of use. However, the lack of a unique solution to the inverse scattering problem prevents its use in a large number of applications. Improvements in the interpretation of scattered light should therefore enable optical scattering techniques to be employed in new quality control applications.

The full strength of optical scattering lies in its ability to diagnose deviations from ideal conditions. For example, optical scattering from smooth surfaces, such as mirrors, transparent optics, and silicon wafers, can yield information about the condition of those surfaces. Surface roughness, particulate contamination, and subsurface defects result from adverse conditions in a manufacturing environment, and distinguishing them should result in improvements in the ability to identify the sources of such conditions.

Because a particle that is smaller than the wavelength of the light scatters in free space with an efficiency proportional to the sixth power of its diameter, detection of small particles quickly becomes limited by whatever other sources of optical scatter exist, such as microroughness. Reduction of the microroughness-induced scatter thus improves the detection of these small particles. Out-of-plane scattering is believed to allow the discrimination between scattering resulting from particulate contamination and surface roughness.[1–3] Polarization techniques have also been employed to distinguish different scattering mechanisms.[4]

In this paper we explore polarized out-of-plane scattering that results from small spheres above (particles) and below (defects) a surface. We find that the polarization of scattered light is different for particulate contaminants, subsurface defects, and surface microroughness. In fact, there exist directions for each of these three mechanisms for which $p$-polarized light will not radiate when $p$-polarized light is incident on the sample. By one viewing the sample in these configurations, the signal from one of the sources of scatter can be removed. We present results of experimental measurements that demonstrate this behavior in separate publications.[5,6]

## 2. Theory

We review the theory originally presented by Videen *et al.*[7–9] to calculate the angular dependence and polarization of light scattered by a particle of refractive

The author is with the Optical Technology Division, National Institute of Standards and Technology, Gaithersburg, Maryland 20899.

Received 7 May 1997; revised manuscript received 28 July 1997.

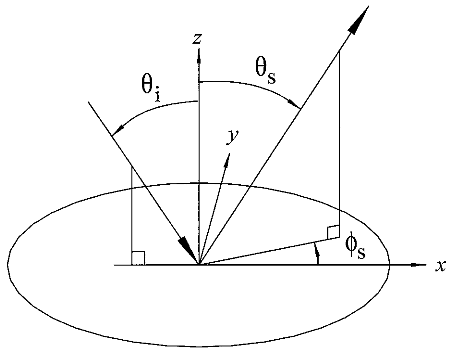


Fig. 1. Measuring geometry defining the angles $\theta_i$, $\theta_s$, and $\phi_s$.

index $n_{\text{sph}}$ having radius $a$, located a distance $d$ from a surface of a material with refractive-index $n_{\text{mat}}$. The refractive indices may be complex, with nonnegative imaginary components. We restrict the discussion to particles sufficiently small compared with the wavelength so that the Rayleigh approximation can be used throughout. Furthermore, multiple interactions with the particle are ignored, even when the particle is close to the interface. This approximation should be valid for sufficiently small particles.

Figure 1 shows the measuring geometry used for this discussion. Plane-wave polarized light of wavelength $\lambda$ irradiates the surface and the particle at an incident angle of $\theta_i$. We are interested in solving for the radiance that is scattered into a direction defined by a polar angle $\theta_s$ and an out-of-plane angle $\phi_s$. The scattering (Jones) matrix $S$ is defined as the relationship between the incident and scattered fields:

$$\begin{pmatrix} E_p^{\text{scat}} \\ E_s^{\text{scat}} \end{pmatrix} = \frac{\exp(ikR)}{R} \begin{pmatrix} S_{pp} & S_{sp} \\ S_{ps} & S_{ss} \end{pmatrix} \begin{pmatrix} E_p^{\text{inc}} \\ E_s^{\text{inc}} \end{pmatrix}, \tag{1}$$

where $R$ is the distance from the scatterer to the detector and $k = 2\pi/\lambda$. It is the purpose of this discussion to calculate the matrix $S$. The bidirectional reflectance distribution function (BRDF) is then related to the scattered field from a single particle or defect by[10]

$$\text{BRDF} = \frac{N}{A} \frac{|S \cdot \hat{\mathbf{e}}|^2}{\cos\theta_s \cos\theta_i} F, \tag{2}$$

where $N/A$ is the density of scatterers within the illuminated area, $\hat{\mathbf{e}}$ is a unit vector parallel to the incident electric field, and $F$ is a structure factor that depends on the correlation between different scattering centers. For random and uncorrelated particles, $F = 1$.

We calculate the scattered light fields in the following manner. First, the electric field $\mathbf{E}$ at the location of the particle is determined in the absence of the particle. Then we determine the dipole moment of the particle $\mathbf{P}_{\text{sphere}}$ assuming that the particle is a sphere, so that[11]

$$\mathbf{P}_{\text{sphere}} = 4\pi\epsilon_0 \frac{n_{\text{sph}}^2 - n_0^2}{n_{\text{sph}}^2 + 2n_0^2} a^3 \mathbf{E}, \tag{3}$$

where $n_0$ is the refractive index of the surrounding medium. This induced dipole is then assumed to radiate according to[11]

$$\mathbf{E}^{\text{scat}} = -\frac{n_0^2 k^2 \exp(in_0 kR)}{4\pi\epsilon_0 R} \hat{\mathbf{k}} \times (\hat{\mathbf{k}} \times \mathbf{P}_{\text{sphere}}), \tag{4}$$

where $\hat{\mathbf{k}}$ is a unit vector in the direction of the radiating light (toward the detector). A coordinate system is chosen in each case discussed below so that the field can be expressed with respect to a right-handed coordinate system defined by the basis set $\{\hat{\mathbf{s}}, \hat{\mathbf{p}}, \hat{\mathbf{k}}\}$ that allows separation of the $p$- and $s$-polarized fields. That is, $\hat{\mathbf{k}}$ is a unit vector in the direction of propagation of the scattered light, $\hat{\mathbf{s}}$ is a unit vector perpendicular to $\hat{\mathbf{k}}$ and parallel to the surface plane, and $\hat{\mathbf{p}} = \hat{\mathbf{k}} \times \hat{\mathbf{s}}$. It is then straightforward to show that

$$\mathbf{E}^{\text{scat}} = \frac{n_0^2 k^2 \exp(in_0 kR)}{4\pi\epsilon_0 R} (\hat{\mathbf{p}}\hat{\mathbf{p}} + \hat{\mathbf{s}}\hat{\mathbf{s}}) \cdot \mathbf{P}_{\text{sphere}}. \tag{5}$$

We can calculate the interaction with a plane interface by taking the inner product (from the left) of the field with an appropriate operator. The refraction operator for a plane wave traveling from region $i$ to region $j$ is then

$$t_p^{ij}(\theta_i)\hat{\mathbf{p}}_j\hat{\mathbf{p}}_i + t_s^{ij}(\theta_i)\hat{\mathbf{s}}_j\hat{\mathbf{s}}_i, \tag{6}$$

where $\hat{\mathbf{p}}_i$ and $\hat{\mathbf{s}}_i$ are the unit vectors appropriate for describing the light before refraction, $\hat{\mathbf{p}}_j$ and $\hat{\mathbf{s}}_j$ are the unit vectors appropriate for describing the light after refraction, and $\theta_i$ is the angle of incidence of the light in region $i$. The Fresnel transmission coefficients $t_p^{ij}(\theta_i)$ and $t_s^{ij}(\theta_i)$ for an interface between materials having refractive-indices $n_i$ and $n_j$ are

$$t_s^{ij}(\theta_i) = \frac{2\cos\theta_i}{\cos\theta_i + [(n_j/n_i)^2 - \sin^2\theta_i]^{1/2}},$$

$$t_p^{ij}(\theta_i) = \frac{2(n_j/n_i)\cos\theta_i}{(n_j/n_i)^2\cos\theta_i + [(n_j/n_i)^2 - \sin^2\theta_i]^{1/2}}. \tag{7}$$

The refraction operator for a spherical wave in the far field is (see Appendix A)

$$\frac{n_i}{n_j}\left(\frac{\cos\theta_i}{\cos\theta_j}\right)^{1/2} [t_p^{ij}(\theta_i)\hat{\mathbf{p}}_j\hat{\mathbf{p}}_i + t_s^{ij}(\theta_i)\hat{\mathbf{s}}_j\hat{\mathbf{s}}_i], \tag{8}$$

where it is assumed that the wave propagates as $\exp(in_i kR)/R$ in region $i$. The reflection operator for both plane waves and spherical waves is simply

$$r_p^{ij}(\theta_i)\hat{\mathbf{p}}_j\hat{\mathbf{p}}_i + r_s^{ij}(\theta_i)\hat{\mathbf{s}}_j\hat{\mathbf{s}}_i, \tag{9}$$

where the Fresnel reflection coefficients are given by

$$r_p^{ij}(\theta) = \frac{(n_j/n_i)^2\cos\theta - [(n_j/n_i)^2 - \sin^2\theta]^{1/2}}{(n_j/n_i)^2\cos\theta + [(n_j/n_i)^2 - \sin^2\theta]^{1/2}},$$

$$r_s^{ij}(\theta) = \frac{\cos\theta - [(n_j/n_i)^2 - \sin^2\theta]^{1/2}}{\cos\theta + [(n_j/n_i)^2 - \sin^2\theta]^{1/2}}. \tag{10}$$

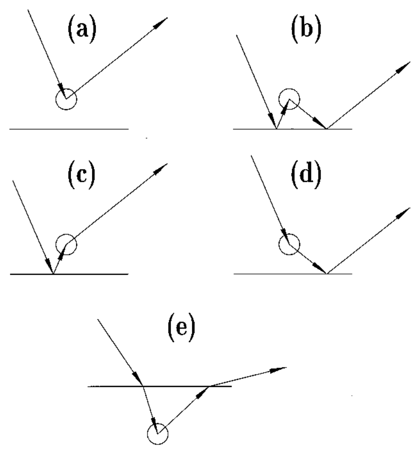

Fig. 2. First-order interactions between light and a sphere (a–d) above a surface and (e) below a surface.

In this paper we assume that light is scattered from the sphere only once. That is, the interaction of the particle or defect with its image in the surface is neglected.

### A. Particle Above the Surface

Figures 2(a)–2(d) show diagrams describing the relevant first-order interactions between light and a particle above a surface. When the particle lies above the surface, it is irradiated from two directions, directly from the source and from the image of the source in the surface. The latter field is decreased and phase shifted by reflection and is also phase shifted as a result of the added path-length $2d \cos \theta_i$ that the light travels upon reflection. Therefore, the electric field at the location of the particle is

$$\begin{aligned}\mathbf{E} = {} & E_p^{\text{inc}}[1 - \alpha r_p^{12}(\theta_i)]\cos \theta_i \hat{\mathbf{x}} \\ & + E_s^{\text{inc}}[1 + \alpha r_s^{12}(\theta_i)]\hat{\mathbf{y}} \\ & + E_p^{\text{inc}}[1 + \alpha r_p^{12}(\theta_i)]\sin \theta_i \hat{\mathbf{z}},\end{aligned} \tag{11}$$

where $E_p^{\text{inc}}$ ($E_s^{\text{inc}}$) is the $p$- ($s$)-polarized component of the incident electric field, $\alpha = \exp(2ikd \cos \theta_i)$ is the phase associated by the path-length difference (and with respect to the superscripts on the reflection coefficients), region 1 is the region above the surface, and region 2 is the region below the surface. The dipole moment of the particle is then given by Eq. (3) with $n_0 = 1$. The orthogonal basis vectors used to describe the scattered electric field are

$$\begin{aligned}\hat{\mathbf{s}}_{\text{scat}} &= -\sin \phi_s \hat{\mathbf{x}} + \cos \phi_s \hat{\mathbf{y}}, \\ \hat{\mathbf{p}}_{\text{scat}} &= -\cos \theta_s \cos \phi_s \hat{\mathbf{x}} - \cos \theta_s \sin \phi_s \hat{\mathbf{y}} + \sin \theta_s \hat{\mathbf{z}}, \\ \hat{\mathbf{k}}_{\text{scat}} &= \sin \theta_s \cos \phi_s \hat{\mathbf{x}} + \sin \theta_s \sin \phi_s \hat{\mathbf{y}} + \cos \theta_s \hat{\mathbf{z}}.\end{aligned} \tag{12}$$

Similarly, the orthogonal basis vectors appropriate for the field that will reflect into $\{\hat{\mathbf{s}}_{\text{scat}}, \hat{\mathbf{p}}_{\text{scat}}, \hat{\mathbf{k}}_{\text{scat}}\}$ are

$$\begin{aligned}\hat{\mathbf{s}}_{\text{rfl}} &= -\sin \phi_s \hat{\mathbf{x}} + \cos \phi_s \hat{\mathbf{y}}, \\ \hat{\mathbf{p}}_{\text{rfl}} &= \cos \theta_s \cos \phi_s \hat{\mathbf{x}} + \cos \theta_s \sin \phi_s \hat{\mathbf{y}} + \sin \theta_s \hat{\mathbf{z}}, \\ \hat{\mathbf{k}}_{\text{rfl}} &= \sin \theta_s \cos \phi_s \hat{\mathbf{x}} + \sin \theta_s \sin \phi_s \hat{\mathbf{y}} - \cos \theta_s \hat{\mathbf{z}}.\end{aligned} \tag{13}$$

Applying Eqs. (5) and (9), we can give the radiation in the far field by

$$\begin{aligned}\mathbf{E}^{\text{scat}} = {} & \frac{k^2 \exp(ikR)}{4\pi\epsilon_0 R}[\hat{\mathbf{p}}_{\text{scat}}\hat{\mathbf{p}}_{\text{scat}} + \hat{\mathbf{s}}_{\text{scat}}\hat{\mathbf{s}}_{\text{scat}} \\ & + \beta r_p^{12}(\theta_s)\hat{\mathbf{p}}_{\text{scat}}\hat{\mathbf{p}}_{\text{rfl}} + \beta r_s^{12}(\theta_s)\hat{\mathbf{s}}_{\text{scat}}\hat{\mathbf{s}}_{\text{rfl}}] \cdot \mathbf{P}_{\text{sphere}},\end{aligned} \tag{14}$$

where $\beta = \exp(2ikd \cos \theta_s)$ accounts for the path-length difference between the light directly radiated by the particle and that reflected from the surface. Simplifying the expressions, we arrive at the scattering matrix elements $S_{ij}^{\text{part}} = q_{ij}^{\text{part}} S_0^{\text{part}}$, where

$$S_0^{\text{part}} = \left(\frac{n_{\text{sph}}^2 - 1}{n_{\text{sph}}^2 + 2}\right) a^3 k^2, \tag{15}$$

$$\begin{aligned}q_{ss}^{\text{part}} &= [1 + \beta r_s^{12}(\theta_s)][1 + \alpha r_s^{12}(\theta_i)]\cos \phi_s, \\ q_{sp}^{\text{part}} &= -[1 - \beta r_p^{12}(\theta_s)][1 + \alpha r_s^{12}(\theta_i)]\cos \theta_s \sin \phi_s, \\ q_{ps}^{\text{part}} &= -[1 + \beta r_s^{12}(\theta_s)][1 - \alpha r_p^{12}(\theta_i)]\cos \theta_i \sin \phi_s, \\ q_{pp}^{\text{part}} &= [1 + \beta r_p^{12}(\theta_s)][1 + \alpha r_p^{12}(\theta_i)]\sin \theta_i \sin \theta_s \\ & \quad - [1 - \beta r_p^{12}(\theta_s)][1 - \alpha r_p^{12}(\theta_i)]\cos \theta_s \cos \theta_i \cos \phi_s.\end{aligned} \tag{16}$$

From Eq. (2), the BRDF for a smooth surface covered with a density $N/A$ of such particles is

$$\begin{aligned}\text{BRDF}_{\text{part}} = {} & \frac{16\pi^4}{\lambda^4}\left(\frac{n_{\text{sph}}^2 - 1}{n_{\text{sph}}^2 + 2}\right)^2 \frac{a^6}{\cos \theta_s \cos \theta_i}\frac{NF}{A} \\ & \times |q_{ij}^{\text{part}} \cdot \hat{\mathbf{e}}|^2.\end{aligned} \tag{17}$$

In the limit of a perfectly conducting surface, so that $n_{\text{mat}} \to \infty(1 + i)$, and for $d \to 0$, the elements $q_{ss}^{\text{part}}$, $q_{sp}^{\text{part}}$, and $q_{ps}^{\text{part}}$ vanish with order $d^2$ as $d \to 0$ and $q_{pp}^{\text{part}} \to 4 \sin \theta_i \sin \theta_s$.

### B. Defect Below the Surface

Figure 2(e) shows the relevant first-order interactions for light interacting with a sphere below a surface. When the particle or defect is located a distance $d$ below the surface, it is illuminated by only one source, and the detector only views the particle or defect from one direction. However, because of refraction, the defect is illuminated from a different direction than that of the incident light, and the radiated light must be converted appropriately into the viewing coordinate system. The fields local to the particle or defect can be expressed as

$$\mathbf{E} = E_p^{\text{inc}}\gamma t_p^{12}(\theta_i)\cos\theta_i'\hat{\mathbf{x}} + E_s^{\text{inc}}\gamma t_s^{12}(\theta_i)\hat{\mathbf{y}} + E_p^{\text{inc}}\gamma t_p^{12}(\theta_i)\sin\theta_i'\hat{\mathbf{z}}, \tag{18}$$

where the angles $\theta_i'$ and $\phi_i'$ are the complex internal angles upon refraction so that

$$\sin\theta_i' = \frac{1}{n_{\text{mat}}}\sin\theta_i,$$
$$\cos\theta_i' = \frac{1}{n_{\text{mat}}}(n_{\text{mat}}^2 - \sin^2\theta_i)^{1/2}, \tag{19}$$

and $\gamma = \exp(in_{\text{mat}}kd\cos\theta_i')$ is a phase factor that accounts for the propagation and absorption of light from the interface to the defect. The induced dipole moment is given by Eq. (3) with $n_0 = n_{\text{mat}}$. The scattered light can then be expressed naturally with respect to the orthogonal basis set:

$$\hat{\mathbf{s}}_{\text{sub}} = -\sin\phi_s'\hat{\mathbf{x}} + \cos\phi_s'\hat{\mathbf{y}},$$
$$\hat{\mathbf{p}}_{\text{sub}} = -\cos\theta_s'\cos\phi_s'\hat{\mathbf{x}} - \cos\theta_s'\sin\phi_s'\hat{\mathbf{y}} + \sin\theta_s'\hat{\mathbf{z}},$$
$$\hat{\mathbf{k}}_{\text{sub}} = \sin\theta_s'\cos\phi_s'\hat{\mathbf{x}} + \sin\theta_s'\sin\phi_s'\hat{\mathbf{y}} + \cos\theta_s'\hat{\mathbf{z}}, \tag{20}$$

which transforms into the basis set in Eq. (12) upon refraction. Once again, the angles $\theta_s'$ and $\phi_s'$ are the complex internal angles upon refraction so that

$$\sin\theta_s' = \frac{1}{n_{\text{mat}}}\sin\theta_s,$$
$$\cos\theta_s' = \frac{1}{n_{\text{mat}}}(n_{\text{mat}}^2 - \sin^2\theta_s)^{1/2}, \tag{21}$$

and $\phi_s' = \phi_s$. Applying Eqs. (5) and (8), we obtain the scattered light in the far field outside the material:

$$\mathbf{E}^{\text{scat}} = \frac{n_{\text{mat}}k^2\exp(ikR)}{4\pi\epsilon_0 R}\left(\frac{\cos\theta_s}{\cos\theta_s'}\right)^{1/2} \times [\delta t_p^{21}(\theta_s')\hat{\mathbf{p}}_{\text{scat}}\hat{\mathbf{p}}_{\text{sub}} + \delta t_s^{21}(\theta_s')\hat{\mathbf{s}}_{\text{scat}}\hat{\mathbf{s}}_{\text{sub}}]\cdot\mathbf{P}_{\text{sphere}}, \tag{22}$$

where $\delta = \exp(in_{\text{mat}}kd\cos\theta_s')$. Once again, by our simplifying the above expressions, the scattering elements can be given by $S_{ij}^{\text{sub}} = q_{ij}^{\text{sub}}S_0^{\text{sub}}$, where

$$S_0^{\text{sub}} = 4\delta\gamma\left(\frac{n_{\text{sph}}^2 - n_{\text{mat}}^2}{n_{\text{sph}}^2 + 2n_{\text{mat}}^2}\right)\cos\theta_s\cos\theta_i a^3k^2n_{\text{mat}}^{3/2}\left[\frac{(n_{\text{mat}}^2 - \sin^2\theta_s)^{1/2}}{\cos\theta_s}\right]^{1/2}, \tag{23}$$

$$q_{ss}^{\text{sub}} = \frac{\cos\phi_s}{[\cos\theta_i + (n_{\text{mat}}^2 - \sin^2\theta_i)^{1/2}][\cos\theta_s + (n_{\text{mat}}^2 - \sin^2\theta_s)^{1/2}]},$$
$$q_{sp}^{\text{sub}} = \frac{-\sin\phi_s(n_{\text{mat}}^2 - \sin^2\theta_s)^{1/2}}{[\cos\theta_i + (n_{\text{mat}}^2 - \sin^2\theta_i)^{1/2}][n_{\text{mat}}^2\cos\theta_s + (n_{\text{mat}}^2 - \sin^2\theta_s)^{1/2}]},$$
$$q_{ps}^{\text{sub}} = \frac{-\sin\phi_s(n_{\text{mat}}^2 - \sin^2\theta_i)^{1/2}}{[n_{\text{mat}}^2\cos\theta_i + (n_{\text{mat}}^2 - \sin^2\theta_i)^{1/2}][\cos\theta_s + (n_{\text{mat}}^2 - \sin^2\theta_s)^{1/2}]},$$
$$q_{pp}^{\text{sub}} = \frac{\sin\theta_i\sin\theta_s - (n_{\text{mat}}^2 - \sin^2\theta_i)^{1/2}(n_{\text{mat}}^2 - \sin^2\theta_s)^{1/2}\cos\phi_s}{[n_{\text{mat}}^2\cos\theta_i + (n_{\text{mat}}^2 - \sin^2\theta_i)^{1/2}][n_{\text{mat}}^2\cos\theta_s + (n_{\text{mat}}^2 - \sin^2\theta_s)^{1/2}]}. \tag{24}$$

The BRDF for subsurface defects or particles is given by

$$\text{BRDF}_{\text{sub}} = \frac{256\pi^4}{\lambda^4}\left(\frac{n_{\text{sph}}^2 - n_{\text{mat}}^2}{n_{\text{sph}}^2 + 2n_{\text{mat}}^2}\right)^2 a^6\cos\theta_i(n_{\text{mat}}^2 - \sin^2\theta_s)^{1/2}|\gamma\delta|^2 n_{\text{mat}}^3\frac{NF}{A} \times |q_{ij}^{\text{sub}}\cdot\hat{\mathbf{e}}|^2. \tag{25}$$

Note that $|\gamma\delta|^2$ accounts for the penetration depth of the material so that defects far below the surface are not observed when the material is absorbing.
oughness-Induced Scatter

To compare these results with those for microroughness-induced scatter in the smooth surface limit, we summarize the results of first-order vector perturbation (Rayleigh–Rice) theory.[12–14] Assuming that the power spectral density (PSD) of the surface is given by $S(\mathbf{f})$, where $\mathbf{f}$ is a two-dimensional spatial frequency, we can give the bidirectional reflectance distribution function by

$$\text{BRDF}_{\text{topo}} = \frac{16\pi^2}{\lambda^4}\cos\theta_i\cos\theta_s S(\mathbf{f}) \times |q_{ij}^{\text{topo}}\cdot\hat{\mathbf{e}}|^2, \tag{26}$$

where the $q_{ij}^{\text{topo}}$ are given by

$$q_{ss}{}^{\text{topo}} = \frac{(n_{\text{mat}}{}^2 - 1)\cos\phi_s}{[\cos\theta_i + (n_{\text{mat}}{}^2 - \sin^2\theta_i)^{1/2}][\cos\theta_s + (n_{\text{mat}}{}^2 - \sin^2\theta_s)^{1/2}]},$$

$$q_{sp}{}^{\text{topo}} = \frac{-(n_{\text{mat}}{}^2 - 1)\sin\phi_s(n_{\text{mat}}{}^2 - \sin^2\theta_s)^{1/2}}{[\cos\theta_i + (n_{\text{mat}}{}^2 - \sin^2\theta_i)^{1/2}][n_{\text{mat}}{}^2\cos\theta_s + (n_{\text{mat}}{}^2 - \sin^2\theta_s)^{1/2}]},$$

$$q_{ps}{}^{\text{topo}} = \frac{-(n_{\text{mat}}{}^2 - 1)\sin\phi_s(n_{\text{mat}}{}^2 - \sin^2\theta_i)^{1/2}}{[n_{\text{mat}}{}^2\cos\theta_i + (n_{\text{mat}}{}^2 - \sin^2\theta_i)^{1/2}][\cos\theta_s + (n_{\text{mat}}{}^2 - \sin^2\theta_s)^{1/2}]},$$

$$q_{pp}{}^{\text{topo}} = \frac{(n_{\text{mat}}{}^2 - 1)[n_{\text{mat}}{}^2\sin\theta_i\sin\theta_s - (n_{\text{mat}}{}^2 - \sin^2\theta_i)^{1/2}(n_{\text{mat}}{}^2 - \sin^2\theta_s)^{1/2}\cos\phi_s]}{[n_{\text{mat}}{}^2\cos\theta_i + (n_{\text{mat}}{}^2 - \sin^2\theta_i)^{1/2}][n_{\text{mat}}{}^2\cos\theta_s + (n_{\text{mat}}{}^2 - \sin^2\theta_s)^{1/2}]}, \tag{27}$$

and the spatial frequency vector **f** is related to $\theta_i$, $\theta_s$, and $\phi_s$ by the Bragg relations:

$$\lambda f_x = \sin\theta_s\cos\phi_s - \sin\theta_i,$$
$$\lambda f_y = \sin\theta_s\sin\phi_s. \tag{28}$$

For $\theta_i = \theta_s = \theta$ and $\phi_s = 0$, the factors $q_{ss}{}^{\text{topo}}$ and $q_{ss}{}^{\text{topo}}$ converge to the specular reflectivities $r_s(\theta)$ and $r_p(\theta)$, respectively.

## 3. Results and Discussion

### A. Relation to Previous Results

Particle scattering from smooth surfaces has been investigated previously in the Rayleigh limit[7,15] and for larger spheres.[8,9,15–21] Aside from our expressing the calculated scatter distributions in terms of a polarized BRDF, the results presented here are similar to the previous results for Rayleigh particles. However, there are some differences, which we discuss briefly in this section.

The results for the scattering from a small sphere above a surface match those of previous reports[7,8] when one considers the slightly different coordinate systems used. In this paper we are careful to maintain a $\{\hat{\mathbf{s}}, \hat{\mathbf{p}}, \hat{\mathbf{k}}\}$ right-handed basis set for all waves and to use the reflection coefficients befitting these bases. It is common, however, to use a different coordinate system for which the coordinate system describing the exitant wave has a different handedness than that of the incident wave; the result is a sign difference in $r_p$ with respect to the present results and a sign difference in one of the columns or rows of the scattering matrix. Consistency between the input and scattering coordinate systems ensures that the scattering matrix signature in the absence of a sample is always the unit matrix.

The results for the scattering from a sphere below a surface differ from those derived previously.[9] The previous result did not evaluate the field far from the sample and therefore did not account for the changing divergence of the light upon refraction. The implications of this distinction is important in Subsection 3.C below.

### B. Polarization of Light Scattered Out of the Plane of Incidence

Previous studies have only evaluated the results for the case of in-plane scattering.[7–9,15–21] We demonstrate here that the out-of-plane scattering signatures for the three mechanisms discussed above are vastly different and potentially allow a means for experimentally separating these contributions in a material.

In Section 2 we intentionally separated terms $q_{ij}$ that have a dependence on the polarization. A comparison of Eqs. (16), (24), and (27) yields nothing extraordinary about the $q_{ss}$, $q_{ps}$, and $q_{sp}$ terms for either the particle scattering, subsurface defect scattering, or topographic scattering. Each of these terms has an identical functional dependence on $\phi_s$, being either $\cos\phi_s$ (for $q_{ss}$) or $\sin\phi_s$ (for $q_{sp}$ and $q_{ps}$). Thus, for these input/output polarization combinations, the contributions from the different scattering mechanisms cannot be distinguished easily by one viewing out of the plane of incidence.

However, the functional forms for $q_{pp}$ differ substantially. Figure 3 shows $|q_{pp}{}^{\text{part}}|^2$, $|q_{pp}{}^{\text{sub}}|^2$, and $|q_{pp}{}^{\text{topo}}|^2$ as functions of $\phi_s$ for input and output angles of $\theta_i = \theta_s = 45°$ and a substrate refractive index that is appro-

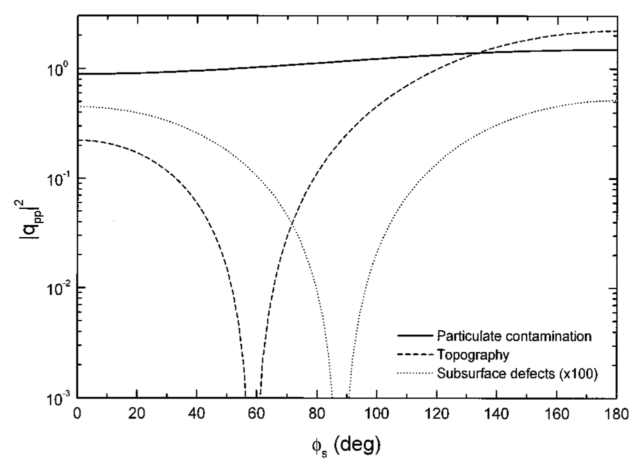


Fig. 3. $|q_{pp}|^2$ factors for a sphere above a surface ($d = 0$), below a surface, and for microroughness as functions of the azimuthal angle $\phi_s$. The incident angle $\theta_i$ and viewing angle $\theta_s$ are both 45°. The substrate material is assumed to be silicon ($n_{\text{mat}} = 3.882 + 0.012i$) at $\lambda = 633$ nm.

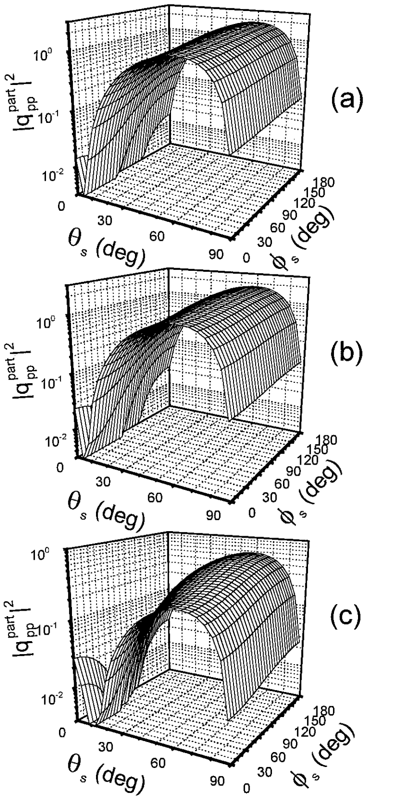


Fig. 4. $|q_{pp}^{\text{part}}|^2$ factors for a sphere above a silicon surface ($d = 0$, $n_{\text{mat}} = 3.882 + 0.012i$) as a function of $\theta_s$ and $\phi_s$ for three incident angles: (a) $\theta_i = 70°$, (b) $\theta_i = 45°$, and (c) $\theta_i = 20°$.

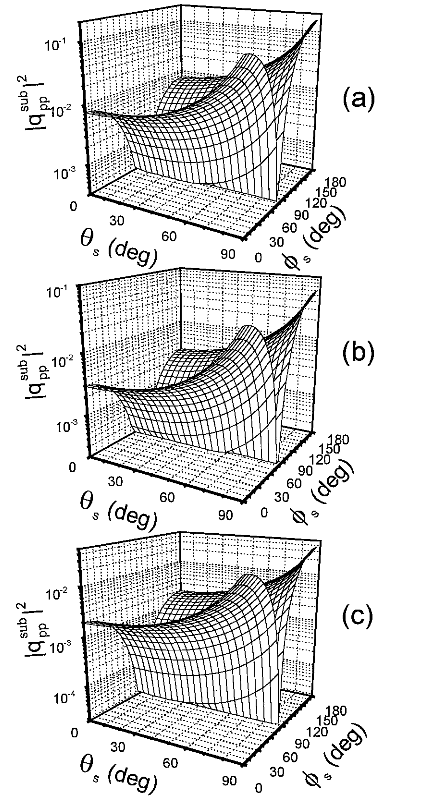


Fig. 5. $|q_{pp}^{\text{sub}}|^2$ factors for a sphere below a silicon surface ($n_{\text{mat}} = 3.882 + 0.012i$) as a function of $\theta_s$ and $\phi_s$ for three incident angles: (a) $\theta_i = 70°$, (b) $\theta_i = 45°$, and (c) $\theta_i = 20°$.

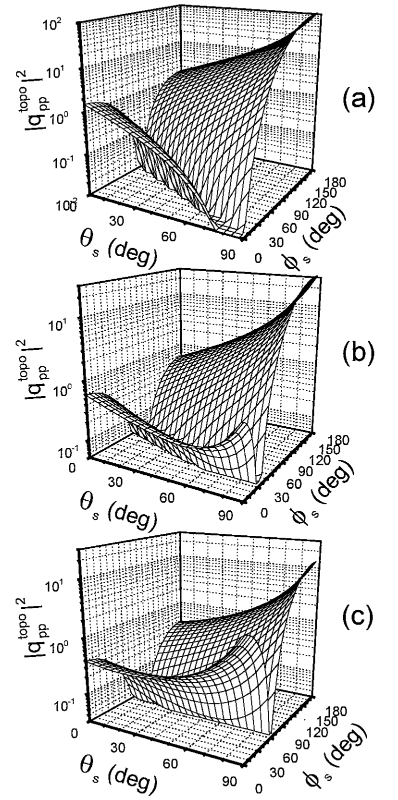


Fig. 6. $|q_{pp}^{\text{topo}}|^2$ factors for a microrough silicon surface ($n_{\text{mat}} = 3.882 + 0.012i$) as a function of $\theta_s$ and $\phi_s$ for three incident angles: (a) $\theta_i = 70°$, (b) $\theta_i = 45°$, and (c) $\theta_i = 20°$.

priate for silicon at $\lambda = 633$ nm ($n_{\text{mat}} = 3.882 + 0.012i$). The differences between the $q_{pp}$ are readily apparent. It can be seen from Fig. 3 that there exist out-of-plane angles $\phi_s$ for which $q_{pp}^{\text{topo}}$ or $q_{pp}^{\text{sub}}$ vanish, whereas $q_{pp}^{\text{part}}$ does not. In particular, at $\phi_s = 59°$ and $\phi_s = 87°$, the scattered light from microroughness and subsurface defects vanish, respectively. For $\theta_i = \theta_s = 45°$, there is no out-of-plane angle for which scatter from particles above the surface vanishes.

With use of the refractive index for silicon, Figs. 4, 5, and 6 show the $|q_{pp}|^2$ for the three mechanisms as functions of $\theta_s$ and $\phi_s$, each at three different incident angles: $\theta_i = 20°$, $45°$, and $70°$. All three mechanisms have distinctly different behavior. At nearly all incident angles $\theta_i$ and scattering angles $\theta_s$, *pp* scattering from small particles is nearly constant in $\phi_s$. Subsurface defect scattering, in contrast, has a marked decrease near $\phi_s = 90°$; the relatively constant angle $\phi_s$ with $\theta_i$ and $\theta_s$ is a result of the large index of refraction of silicon. For microroughness-induced scatter, the azimuthal angle $\phi_s$ at which $|q_{pp}^{\text{topo}}|^2$ vanishes depends strongly on the incident and scattering angles $\theta_i$ and $\theta_s$. It can be seen that this behavior is a bidirectional equivalent of Brewster's angle because the trough in Fig. 6 moves toward the specular direction $\theta_s = \theta_i$ and $\phi_s = 0$ as the incident angle moves toward Brewster's angle $\theta_B = 75.6°$.

There are combinations of $\theta_i$ and $\theta_s$ for which a scattering null $\phi_s$ exists for each of the scattering mechanisms. Figure 7 shows the out-of-plane angle $\phi_s$ for which a null occurs for each combination of $\theta_i$ and $\theta_s$, for each of the scattering mechanisms, and for two different materials: silicon and glass. The curves display combinations of $\theta_i$ and $\theta_s$ for which a scattering null exists by showing curves of constant $\phi_s$ where the null occurs.

The theory becomes more complex as the particle size restriction is lifted, and the Rayleigh limit is no longer valid. However, the contributions from the topographic scattering will not change under these conditions, and the scattering from particles is not expected to develop minima in the same region. The model assumed that the particles are spherically symmetric, both in their size and shape as well as in their microscopic structure. For nonspherically symmetric particles, the induced dipole moment cannot be expected to be parallel to the applied electric field. Thus the theory will require modifications for particles that are birefringent, nonspherical, or magnetic.

The expressions in Eqs. (16), (24), and (27) are all written as Jones matrices, implying that no light is depolarized. However, the models for particles and defects imply that all $N$ particles and defects are identical in the sampling area $A$. Because the polarization terms $q_{ij}^{\text{part}}$ depend on $d$, a distribution of particle sizes will give rise to some depolarization of the scattered light (since $d = a$ for a particle attached to the surface). However, the distribution of heights for which the Rayleigh approximation is valid should be sufficiently small that depolarization can be neglected. Nonspherical particles will lead to depolarization since their orientations will be random. Because $q_{ij}^{\text{sub}}$ is independent of $d$, a distribution of defect depths should not depolarize the scattered light. However, as with particles above a surface, a random distribution of nonspherical defects would lead to depolarization of the scattered light. To the first order, light scattered by microroughness is not expected to lead to depolarization.

### C. Use of Wavelength Scaling to Determine the Scattering Mechanism

The results of the above calculations have some profound implications on the current practice of using wavelength scaling to deduce the mechanism by which light is scattered in a particular sample.[22] BRDF's measured at a number of different wavelengths are often converted to the PSD of the surface roughness with Eqs. (26)–(28). If the curves lie upon each other, then the results are interpreted as indicating that the light is indeed resulting predominantly from scattering from surface microroughness and not from another mechanism such as subsurface defects, particulate contamination, or grain boundaries. We point out that this practice can be misleading, especially if the measurements are only carried out in the plane of incidence or with $s$-polarized incident light.

A comparison of the results from microroughness-induced scatter with those from subsurface defects yields striking similarities between the angle and wavelength dependences. The BRDF from both mechanisms can be considered to be the product of four factors: a Rayleigh blue sky factor with the $1/\lambda^4$ dependence, an obliquity factor having the product of the cosines of incident and viewing angles, a structure factor [$\mathbf{F}$ in Eq. (25) and $S(\mathbf{f})$ in Eq. (26)], a polarizability factor [the $a^6|(n_{\text{sph}}^2 - n_{\text{mat}}^2)/(n_{\text{sph}}^2 + 2n_{\text{mat}}^2)|^2$ factor in Eq. (25) and the $n_{\text{mat}}^2 - 1$ factor in Eq. (27)], and a polarization-dependent factor (the $q$ factors).

The $q_{ss}$, $q_{sp}$, and $q_{ps}$ are identical for the mechanisms (with the exception of the $n_{\text{mat}}^2 - 1$ factor, which by convention is included in the microroughness-induced terms). The $q_{pp}$ are similar for the two mechanisms, but not identical. The obliquity factors are nearly the same, except that, for subsurface defects, the applicable scattering angle is the internal angle $\theta_s'$ instead of the external angle $\theta_s$.

Although we have not explicitly written out the structure factor for subsurface defects, it is expected to have a form similar to that for microroughness. That is, defects in many systems are likely to have correlations with each other and be expressible with a power spectrum. Correlations of a given spatial frequency in the surface plane will diffract into the same angles as those for the same spatial frequency of surface microroughness with use of Eq. (28). Furthermore, the defects are likely to exist near the surface and therefore follow the topography, making power spectra for the subsurface defects and the topography behave similarly.

The obliquity factor has a minor effect on the BRDF except at large scattering angles, where subsurface scattering would cause an upturning in the data at large spatial frequencies if it were misrepresented as resulting from microroughness. This upturning is commonly observed in the reported PSD for a wide variety of surfaces, is usually left unexplained, and always causes deviations from the PSD's measured with different wavelengths.[22]

The polarizability terms, of course, are different since the scattering sources are different. Depending on the type of subsurface defect, this term may have a strong wavelength dependence or a weak one. If the defect has a refractive index close to that of the host material, then small changes in one wavelength dependence compared with the other can cause relatively large changes in the polarizability of the defect. However, if the defect has a refractive index much different than the host material, then one might expect that the wavelength dependence of the polarizability can be similar to that of the microroughness. In fact, if the defect is a void having an index $n_{\text{sph}} = 1$, then the polarizability associated with the defect has a functional dependence similar to that associated with microroughness.

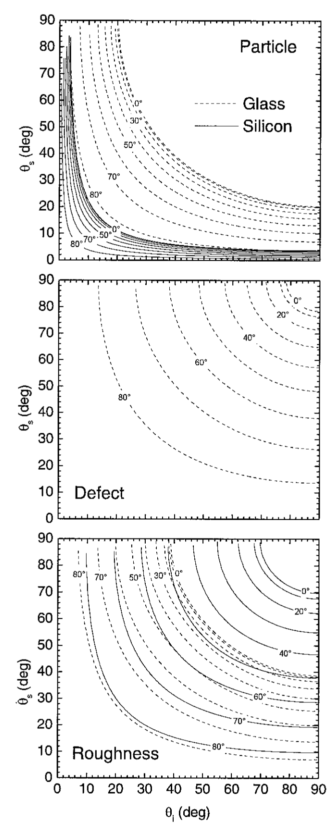


Fig. 7. Curves of constant azimuthal angle $\phi_s$ for which zeros exist in $q_{pp}$, plotted in the $\theta_i$–$\theta_s$ plane for scattering from particles, subsurface defects, and microroughness. The functions are evaluated with the refractive indices for glass ($n_{\text{mat}} = 1.4$) and silicon ($n_{\text{mat}} = 3.882 + 0.012i$). For ($\theta_i$, $\theta_s$) to the upper right of each $\phi_s = 0$ curve there exist no zeros in the $q_{pp}$. The $\phi_s = 90°$ curve is identical to the $\theta_i$ and $\theta_s$ axes. For defects on silicon, the angles $\phi_s$ are always greater than 80°, so the contours are not shown. For scattering from particles, $d = 0$.

It has been demonstrated that subsurface defects can lead to wavelength dependences in the BRDF that would mimic those expected from microroughness. From the above points, one must question the correctness of using wavelength scaling when interpreting scatter distributions. Polarization-sensitive measurement of scattering out of the plane of incidence, on the other hand, is much more sensitive to the nature of the material response, since, in effect, it responds to the change in the direction of the induced polarization in relation to the incident electric field, and thus responds to the different reflective and refractive interactions that the light experiences during the scattering process. The search for the existence of nulls in the polarized scattering provides a much stronger test for the verification of topographically induced scatter.

## 4. Summary

We have shown that polarized light scattered from particles above a surface, defects below a surface, and surface microroughness can give rise to different dependences on the out-of-plane scattering angle. Zeros in the scattering functions can be found at different out-of-plane angles for each of the scattering mechanisms, allowing the suppression of light scattered from surface roughness, subsurface scattering, and to a lesser degree, particulate contamination. The common practice of using wavelength scaling to determine the scattering mechanism is questioned on the grounds that in-plane scattering resulting from microroughness and subsurface defects are too similar to allow an unambiguous determination of a mechanism for observed scattering.

## Appendix A: Transmission of a Spherical Wave through a Plane Interface

It is common to use transmission coefficients to relate the field strengths of a plane wave on two sides of an interface. In this Appendix, we derive expressions that relate the far-field transmission of a spherical wave emanating from a point near a planar interface. The issue here is that a spherical wave will change its divergence as it passes through the interface. That is, the solid angle $d\Omega_1 = \sin\theta_1 d\theta_1 d\phi_1$ inside the material refracts into $d\Omega_2 = \sin\theta_2 d\theta_2 d\phi_2$ outside the material. From Snell's law,

$$n_1 \sin\theta_1 = n_2 \sin\theta_2.$$

Differentiating, we obtain

$$n_1 \cos\theta_1 d\theta_1 = n_2 \cos\theta_2 d\theta_2.$$

Therefore (realizing that $\phi_1 = \phi_2$),

$$\begin{aligned} d\Omega_2 &= \sin\theta_2 d\theta_2 d\phi_2 \\ &= \frac{n_1 \sin\theta_1}{n_2}\frac{n_1 \cos\theta_1}{n_2 \cos\theta_2} d\theta_1 d\phi_1 \\ &= \frac{{n_1}^2}{{n_2}^2}\frac{\cos\theta_1}{\cos\theta_2} d\Omega_1. \end{aligned}$$

In the geometrical optics approximation, the intensity of light (and hence the square of the field) along a bundle of rays is inversely proportional to the cross-sectional area of that bundle. Therefore, one would expect an extra factor of $(n_1/n_2)(\cos\theta_1/\cos\theta_2)^{1/2}$ in addition to the transmission coefficient when calculating the field strength in the far field.

I thank C. C. Asmail and E. L. Shirley for many useful comments and discussions leading to these results.

## References

1. P. Burggraaf, "Pursuing advanced metrology solutions," Semicond. Int. **17,** 62–64 (1994).
2. R. S. Howland, "Detecting killer particles on rough surfaces," Semicond. Int. **17,** 164–170 (1994).
3. E. Morita, H. Okuda, and F. Inoue, "Distinguishing COPs from real particles," Semicond. Int. **17,** 156–162 (1994).
4. K. Moriya, A. Yazaki, and K. Hirai, "Detection and identification of near-surface microprecipitates in silicon wafers by laser scattering tomography," Jpn. J. Appl. Phys. Pt. 1 **34,** 5721–5728 (1995).
5. T. A. Germer, C. C. Asmail, and B. W. Scheer, "Polarization of out-of-plane scattering from microrough silicon," Opt. Lett. **22,** 1284–1286 (1997).
6. T. A. Germer and C. C. Asmail, "Bidirectional ellipsometry and its application to the characterization of surfaces," in *Polarization Measurement, Analysis, and Remote Sensing*, D. H. Goldstein and R. A. Chipman, eds., Proc. SPIE **3121,** 173–182 (1997).
7. G. Videen, W. L. Wolfe, and W. S. Bickel, "Light scattering Mueller matrix for a surface contaminated by a single particle in the Rayleigh limit," Opt. Eng. **31,** 341–349 (1992).
8. G. Videen, M. G. Turner, V. J. Iafelice, W. S. Bickel, and W. L. Wolfe, "Scattering from a small sphere near a surface," J. Opt. Soc. Am. A **10,** 118–126 (1993).
9. G. Videen, "Light scattering from a sphere behind a surface," J. Opt. Soc. Am. A **10,** 110–117 (1993).
10. D. S. Flynn and C. Alexander, "Polarized surface scattering expressed in terms of a bidirectional reflectance distribution function matrix," Opt. Eng. **34,** 1646–1650 (1995).
11. M. Born and E. Wolf, *Principles of Optics* (Pergamon, Oxford, England, 1980).
12. G. R. Valenzuela, "Depolarization of EM waves by slightly rough surfaces," IEEE Trans. Antennas Propag. **AP-15,** 552–557 (1967).
13. S. O. Rice, "Reflection of electromagnetic waves from slightly rough surfaces," Commun. Pure Appl. Math. **4,** 351–378 (1951).
14. D. E. Barrick, *Radar Cross Section Handbook* (Plenum, New York, 1970).
15. W. S. Bickel, A. J. Watkins, and G. Videen, "The light-scattering Mueller matrix elements for Rayleigh, Rayleigh-Gans, and Mie spheres," Am. J. Phys. **55,** 559–561 (1987).
16. P. A. Bobbert, J. Vlieger, and R. Greef, "Light reflection from a substrate sparsely seeded with spheres—comparison with an ellipsometric experiment," Physica A **137,** 243–257 (1986).
17. K. B. Nahm and W. L. Wolfe, "Light-scattering models for spheres on a conducting plane: comparison with experiment," Appl. Opt. **26,** 2995–2999 (1987).
18. G. Videen, "Light scattering from a sphere on or near a surface," J. Opt. Soc. Am. A **8,** 483–489 (1991).
19. G. Videen, "Light scattering from a sphere on or near a surface: errata," J. Opt. Soc. Am. A **9,** 844–845 (1992).
20. P. A. Bobbert and J. Vlieger, "Light scattering by a sphere on a substrate," Physica A **137,** 209–242 (1986).
21. D. C. Weber and E. D. Hirleman, "Light scattering signatures of individual spheres on optically smooth conducting surfaces," Appl. Opt. **27,** 4019–4026 (1988).
22. J. C. Stover, *Optical Scattering: Measurement and Analysis* (McGraw-Hill, New York, 1990).